ICAS 2016
30th Congress of the International Council of the Aeronautical Sciences
DCC, Daejeon, Korea : September 25-30, 2016

UNSTEADY AERODYNAMIC INFORMATION EXTRACTION USING FFT-BASED UNSTEADY PRESSURE-SENSITIVE PAINT MEASUREMENT

Kazuyuki Nakakita*
*** Japan Aerospace Exploration Agency**

Keywords: *Unsteady Aerodynamics, Pressure-Sensitive Paint (PSP), FFT*

Abstract

FFT-based unsteady PSP measurement was developed as a signal-to-noise ratio improvement method for small pressure fluctuation measurement in low-speed flow. It was extended to extract various unsteady aerodynamic information, which were not only original power spectrum but coherence and phase delay. Measurement system and data reduction method of the FFT-based unsteady PSP measurement was introduced. Two wind tunnel test applications to NACA0012 and 30P30N models were conducted. Unsteady aerodynamic flow structure in those flow fields were investigated using unsteady aerodynamic information in detail.

1 Introduction

Pressure-Sensitive Paint (PSP) measurement [1] is a global pressure measurement technique. It has already become semi-standard measurement technique in wind tunnel test. JAXA has also equipped the productive PSP system in large industrial wind tunnels and utilized it for various researches and developments [2].

Recently, main interest of PSP applications are moving from steady pressure distribution to unsteady aerodynamics. Since around 2000, fast-response PSPs were developed in JAXA and Purdue University [3-6]. In addition, a high-speed camera was also progressed in the points of photosensitivity, pixel size, number of images, and frame rate. A high-power illumination light source like laser diode and LED in blue, violet, and UV is also progressed. Unsteady PSP measurement has been rapidly developed under progress of these key technologies. Transonic and supersonic applications of unsteady PSP measurement [7-12] have typically large pressure variation so that it is straightforward of conventional PSP measurement. High-speed camera images are processed same method with conventional PSP, then, each PSP result is merged to a movie and used to calculate rms value.

Aeroacoustics is one of recent important topics of aerodynamics. Dipole is dominant in low-speed so that unsteady pressure measurement can contribute to understand aeroacoustic flow field. However, pressure fluctuation in aeroacoustic flow fields are too small for a straightforward unsteady PSP measurement and lower than system noise. Various methods were reported to improve signal-to-noise ratio to reduce detection limit [13,14]. JAXA has developed a fast-Fourier Transform (FFT) based method since 2007 [15] and realized to improve pressure fluctuation detection limit down to about 3 Pa rms using a high-speed camera [16].

FFT-based unsteady PSP data reduction has much potential not only in S/N ratio improvement but to extract aerodynamic information using spectral analysis. Power spectrum, coherence, and phase delay of unsteady pressure fluctuation can be extracted by unsteady PSP data reduction process [17]. In this paper, unsteady PSP measurement system including fast-response PSP and measurement equipments and unsteady PSP data reduction method using FFT were introduced. Then, two low-speed applications of unsteady PSP measurement and their results to extract unsteady flow filed information were described in detail.

2 Unsteady PSP Measurement

2.1 Fast-response PSP

2.1.1 Anodized Aluminum PSP

PSP is a molecular sensor based on oxygen quenching of its luminescence. Typical time response of conventional PSP consisted of luminophore and polymer binder is the order 1 second. For unsteady PSP measurement, it is necessary to use much faster PSP. There are several types of fast-response PSPs for unsteady PSP measurement. Polymer-Ceramic PSP (PC-PSP) is one of the fast response PSPs [11,12,18]. It is a sprayable PSP and flexible for model material. Its difficulty is surface roughness control [11].

Anodized aluminum PSP (AA-PSP) is another fast-response PSP consisted of anodized aluminum layer [3,4]. Model material is limited to aluminum alloy. A1000 and A5000 series are most appropriate to AA-PSP. The surface of anodized aluminum is consisted of small porous cell shown in fig. 1. Luminophore, tris(4,7-diphenylphenanthroline) ruthenium(II) dichloride ($[Ru(dpp)_3]Cl_2$) in this study, directly absorbs on the porous aluminum surface. Hydrophobic treatment using stearic acid [5] is also applied to AA-PSP surface to improve the original hydrophilic surface of anodized aluminum to hydrophobic one to reduce AA-PSP characteristics aging. Static pressure sensitivity of AA-PSP is almost same with conventional PSP and PC-PSP. Temperature dependency of AA-PSP with hydrophobic treatment is almost same with conventional PSP and better than PC-PSP. Surface of AA-PSP is covered by dense anodized aluminum layer and it is smooth structure. Surface roughness of AA-PSP affected to model aerodynamic characteristics is mainly caused by model machining process. Surface roughness of AA-PSP is typically better than PC-PSP.

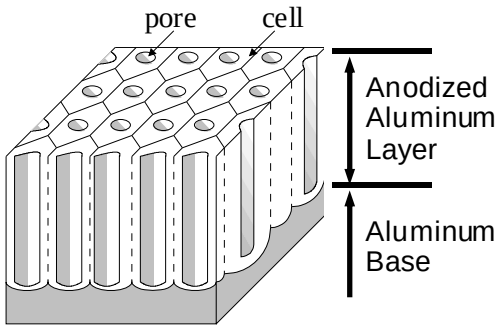

Fig. 1. Schematic drawing of the anodized aluminum layer. Typical thickness of the layer is around 10 μm.

2.1.2 Dynamic Response of AA-PSP

Fig. 4 was a typical dynamic response of an AA-PSP coupon [19] conducted using a speaker and a resonant tube. PSP dynamic response was expressed as the Bode diagram on frequency domain. Gain and phase delay of the AA-PSP was decided by comparison with a Kulite pressure transducer installed on the same AA-PSP coupon. The AA-PSP frequency response at -3dB was 5kHz and the phase delay was 30°. The dynamic response of the AA-PSP was fast enough to this study.

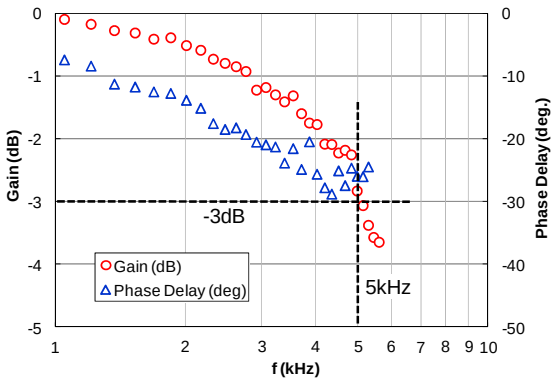

Fig. 2. Typical dynamic response of AA-PSP.

2.2 Unsteady PSP Measurement System

Measurement of the unsteady pressure fluctuation needs at least several times of measurement frequency in practical use. When target phenomena has 1 kHz pressure fluctuation, high-speed camera frame rate should have more than 10 k frame-per-second (fps). High frame-rate measurement reduces exposure time of a high-speed camera. Unsteady PSP measurement system for such high-frequency targets needs to overcome this small exposure time problem. Three solutions were used in present unsteady PSP measurement system;

1. high-performance high-speed camera with high photosensitivity
2. high-power illumination light source

Unsteady PSP measurement system using a high-speed camera in this study was shown in fig. 3. It was consisted of a high-speed camera, a 7W blue laser diode (LD), an illumination collimator, and so on. Main body of 7W blue LD was located out of black curtain in fig. 3. Detail of each components is described below.

2.2.1 High-Speed Camera

The high-speed camera in this system was the Phantom V710 CMOS high-speed video camera (monochrome), which has 12bit depth A/D resolution.

Its sensitivity is ISO 20,000 on newest catalogue. High-sensitivity of a high-speed camera is important for short exposure measurements like unsteady PSP measurement. The phantom V710's maximum spatial resolution is 1280×800 pixels. Maximum number of measurement images are limit by the embedded memory size and S/N ratio of unsteady PSP measurement was due to the number of the images, so that the image size was minimized to the unsteady PSP measurement area to increase total number of the measured images. About 107,000 images (1,000 for dark, 53,000 for wind-off, 53,000 for wind-on) for NACA0012 model test and 99,000 images (1,000 for dark, 48,000 for wind-off, 48,000 for wind-on) for 30P30N model test was acquired for each measurement cases. Frame rate and exposure were 10 kfps and 0.098 ms.

The camera lens was Ai Nikkor 50mm F1.2S due to its maximum brightness in all Nikon lens lineup. Its iris was set to open to collect largest PSP luminescence. The luminescence optical filter, HOYA O58, was set in front of the camera lens to transmit the PSP luminescence wavelength longer than 580nm and cut the illumination light of blue laser.

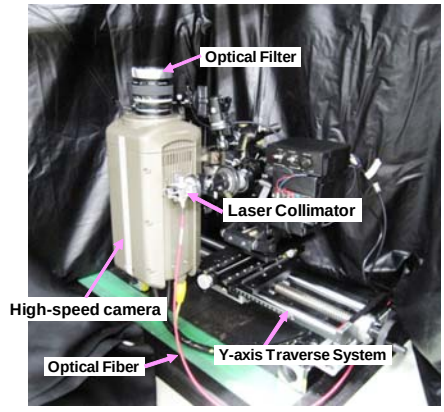

Fig. 3. Unsteady PSP measurement system.

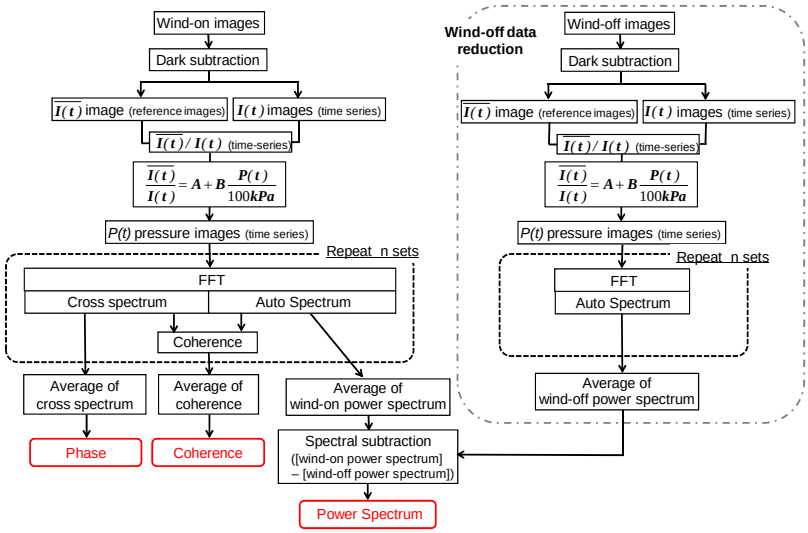

Fig. 4. Flow chart of unsteady PSP data reduction.

2.2.2 Illumination Light Source

To compensate small exposure time, a high-power illumination light source was one of the key components to increase PSP luminescence. The 7W high-power blue LD, Sumitomo Electric Industry BLM-7000-H08D, was used as the illumination light source in this study. It consists of 21 laser diode pieces and their laser lights are bundled to one output. Its wavelength is blue, distributing 450-455 nm, to illuminate Ruthenium base AA-PSP.

Laser light was transmitted through a ϕ0.8mm core optical fiber from the main body of 7W blue LD to the illumination collimator. The collimator was used to adjust the illumination area. Laser light is a point source so that it can be easy controlled its illumination density by changing the collimator focal length. For the unsteady PSP measurement, necessary frame rate, i.e. exposure time, is decide by the target phenomena, so that reasonable camera intensity is produced by the set up of the illumination light source and its illumination density on the model measurement area. When first set up of the collimator gives too small measurement count for the high-speed camera,

illumination density is necessary to be increased by changing collimator set up.

2.3 FFT-Based Data Reduction

To detect small pressure fluctuation in unsteady PSP measurement, noise reduction is important. In steady measurements, data average is simple and powerful method to reduce random noise. However, time-series data of unsteady phenomena cannot be averaged. In this case, introduction of the frequency domain FFT can improve signal-to-noise ratio by averaging [15-17]. Data reduction method of unsteady PSP measurement is based on FFT analysis. Fig. 4 shows the flow chart of FFT based unsteady PSP data reduction. Detail is described below.

2.3.1 Dark Subtraction

All camera images needs to be subtract a dark image. The dark image is acquired under dark environment of unsteady PSP measurement set up without PSP illumination light and PSP luminescence. It includes the other signals like stray light. Subtraction of the dark image from wind-on and wind-off produces effective PSP intensity images.

2.3.2 Pressure Calculation

Pressure calculation in PSP data reduction needs two types of acquired images, which are reference image, I_{ref}, and test image, I. Reference image is PSP intensity image acquired under uniform pressure environment. It is often acquired under atmospheric pressure. The relation between I_{ref}/I and pressure is theoretically represented by following Stern-Volmer relation;

$$\frac{I_{ref}}{I} = A + B\frac{P}{P_{ref}} \qquad (1)$$

Actual PSP characteristics tend to have nonlinear pressure sensitivity so that polynominal expression of eqn.(1) is also used.

For unsteady PSP data reduction to measure small pressure fluctuation around atmospheric pressure in a conventional low-speed wind tunnel, reference image, I_{ref}, in eqn. (1) is possible to assume almost same with time-averaged test images, $\overline{I(t)}$. Reference pressure , P_{ref}, corresponding to atmospheric pressure at the reference image acquisition is also assumed as 100 kPa;

$$I_{ref} \approx \overline{I(t)}, P_{ref} \approx 100kPa \qquad (2)$$

Using eqn. (2), eqn. (1) can be described;

$$\frac{\overline{I(t)}}{I(t)} = A + B\frac{P(t)}{100kPa} \qquad (3)$$

Eqn. (3) is described using only wind-on data. These assumption help to ignore one of the largest problems in low-speed PSP, which is temperature variation between wind-off and wind-on conditions.

Wind-off images were also acquired in wind tunnel test, however, they were used only to compensate the offset noise components on wind-on images described in 2.3.3.1.

2.3.3 Spectral Analysis

Time-series pressure images consisted of *P(t)* map are produced from time-series wind-on images *I(t)* using eqn. (3). Then, spectral analysis was applied. Number of images for the unit of FFT was 2^{10} (=1024) points. 40,000~50,000 time-series pressure images reduced from acquired high-speed camera images were separated to units of 2^9 (=512) images and FFT processing were applied every adjacent two units (=1024 points) with 1/2 overlap to reduce the data loss caused by the Hanning window. Each FFT process produces auto spectrum on each pixel and cross spectrum between reference pixel and each pixel. Power spectrum (or power spectrum density), coherence, and phase delay are reduced using auto and cross spectrum.

2.3.3.1 Power Spectrum

Power spectrum indicates magnitude of unsteady pressure fluctuation along frequency on each pixel. It is calculated from auto spectrum of FFT results. Ensemble average process of power spectrum cannot reduce measurement noise itself, however, can reduce fluctuation of power spectrum. Detection limit of unsteady PSP measurement is decided by the magnitude of this fluctuation. Ensemble average reduces power spectrum fluctuation and improves signal-to-noise ratio. Larger number

of ensemble average corresponds larger S/N ratio improvement.

Power spectrum from wind-on pressure images includes effective aerodynamic fluctuation components and noise ones. Spectral subtraction [20] using wind-off power spectrum is applied to remove noise components. Spectral subtraction is common noise-cancelling technique. Wind-on power spectrum includes pressure fluctuation signals and noise components and one of wind-off includes only noise components so that wind-off power spectrum is used to reduce overlapped noise components. Effective power spectrum after spectral subtraction includes only pressure fluctuation components.

2.3.3.2 Coherence

Coherence indicates magnitude of correlation of pressure behavior between one pixel and reference one on each frequency. It is calculated from auto spectrum of each pixel and cross spectrum between each pixel and reference one on pressure images of FFT results. Largest pressure fluctuation pixel was selected as reference pixel in this study, however, it could replace to unsteady pressure transducer data and so on. Coherence between two locations, X and Y, at frequency f is expressed as follows;

$$Coh^2(f) = \frac{|S_{XY}(f)|^2}{S_{XX}(f)S_{YY}(f)} \qquad (4)$$

where $S_{XY}(f)$ is the cross-spectrum function between the unsteady pressure at two locations, X and Y. S_{XX}, S_{YY} are the auto-spectrum function at X and Y. Coh^2 value takes from 0 to 1. Larger coherence means larger correlation. Ensemble average is also useful to reduce fluctuation on coherence.

2.3.3.3 Phase Delay

Phase delay indicates phase difference between one pixel and reference one on each frequency. It is calculated from cross spectrum of FFT results. Reference pixel was same with calculation of coherence. Phase delay between two locations, X and Y, at frequency f is expressed as follows;

$$\phi_{XY}(f) = tan^{-1}\left(\frac{Q_{XY}(f)}{K_{XY}(f)}\right) \qquad (5)$$

where $K_{XY}(f)$ is the real part of the cross spectrum $S_{XY}(f)$ and $Q_{XY}(f)$ is that of imaginary part. For ensemble average of phase delay over multiple FFT results, complex expression of the cross spectrum of each FFT result is averaged, then, eqn. (5) was calculated from resultant cross spectrum.

3 Test Models

3.1 NACA0012 Model

The 2-dimensional NACA0012 model was shown in fig. 5. Its chord length was 250 mm and span width was 550 mm, which was same with test section width of the wind tunnel. 260 mm width at the center, yellow section in fig. 5, was the AA-PSP coated area. 7 unsteady

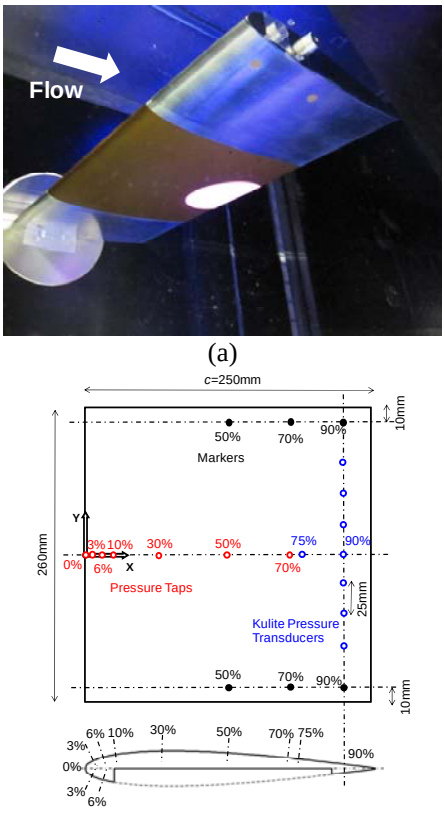

Fig. 5. 2-dimensional NACA0012 model. (a) model installed in JAXA-LWT3. White circle at the trailing edge was the laser illumination area. (b) dimension and pressure tap/transducer arrangement.

pressure transducers were installed at 90% chord location on AA-PSP coated area. White region in fig. 5 at the trailing edge was the area of 7W blue LD illuminated.

The 2-dimensional NACA0012 model was installed in the low-turbulence calibration wind tunnel (LWT3) at JAXA Chofu Aerospace Center. It is a closed circuit with a rectangular test section; 0.55m in width, 0.65m in height, and 1.5m in length. The unsteady PSP measurement system installed on the floor below of the LWT3 test section. PSP tests were conducted in free stream conditions of U=28.0 m/s (P_d=472 Pa). Reynolds number was Re=4.9×10^5 for the model code length c=250 mm.

3.2 30P30N Model

NASA 30P30N airfoil was standard model for Category 7 of the BANC-II Workshop in June, 2012 [21-23]. The deflection angles of both the slat and the flap are equal to 30°. Category 7 under this workshop targeted the slat noise problem on the 30P30N 2-dimensional 3-element high-lift airfoil configuration.

JAXA was manufactured 2-dimensional 30P30N model shown in fig. 6. Its cross section was same, stowed chord=0.4572 m, with NASA 30P30N and span, 2m, was larger than the

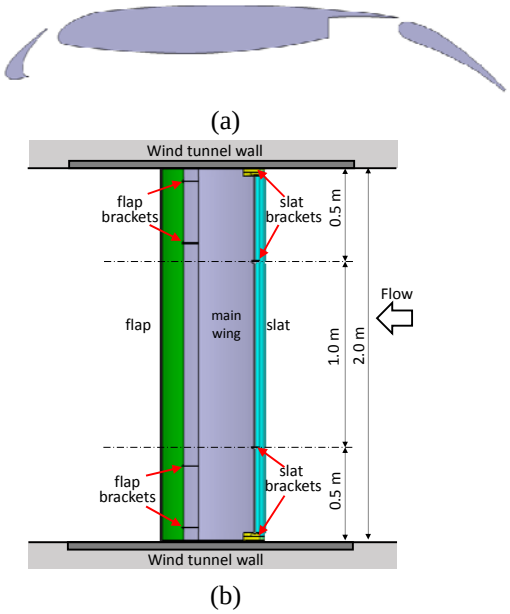

Fig. 6. 2-dimensional 30P30N model. (a) cross-section configuration, (b) schematic view from pressure side.

original NASA one. Its wind tunnel test was conducted in the JAXA-LWT2 [24]. JAXA-LWT2 is an atmospheric pressure, closed-circuit tunnel with a square test section of 2 m in height, 2 m in width, and 4 m in length. Unsteady PSP measurement described in this paper a part of this test campaign. Various another measurements, i.e. static pressure taps, unsteady pressure transducers, and noise source identification via a phased-microphone array, were conducted in a wind tunnel test campaign.

Target of the unsteady PSP measurement was the unsteady flow field on the slat cove so that AA-PSP was coated only on the slat (slat code c_{slat}=68.57mm), which was yellow part in fig. 7. Unsteady PSP measurement area on the slat was the area of blue circle on fig. 7.

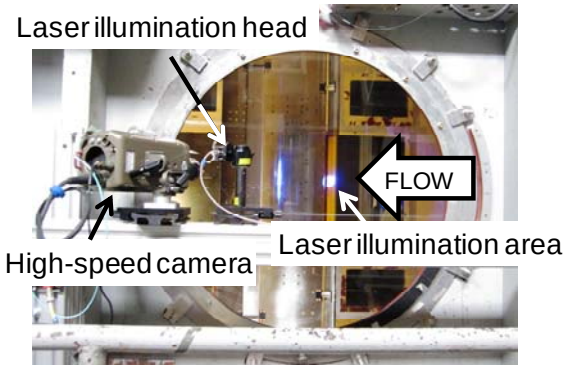

Fig. 7. 30P30N model and unsteady PSP measurement system installed in the LWT2. Measurement area was laser illumination area on the slat.

4 Results and Discussion

4.1 NACA0012 Model

The unsteady PSP measurement of NACA0012 model was conducted for 4 angle of attacks; α=0°, -1.5°, -2.5°, -4.0°. 3 angle of attack cases except α=0° caused trailing edge (T.E.) noise. Results of α=-1.5° and -4.0° were introduced in this paper. Fig. 8 was power spectrum of unsteady pressure transducer data on x/c=0.9 and y/c=0 at α=-1.5°. Fundamental of the unsteady pressure fluctuation was appeared around 920 Hz. It was a pure tonal peak caused by the acoustic feedback between sound wave emitted from the trailing edge and T-S (Tollmien-Schlichting) waves on the pressure

side of the airfoil [25,26]. Magnitude of the time-series pressure fluctuation corresponding to fig. 8 was about 150 Pa peak-to-peak. In NACA0012 case, power spectrum, not power spectrum density (PSD), was used because target phenomena was extremely narrow so that PSD value varied due to the width of Δf.

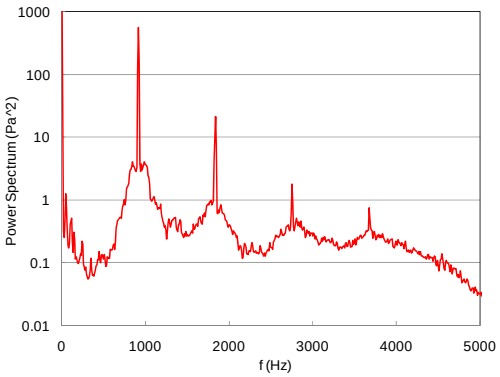

Fig. 8. Power spectrum of NACA0012 at x/c=0.9 and y/c=0 unsteady pressure transducer. α=-1.5°.

Fig. 9 showed unsteady PSP measurement results of fundamental on NACA 0012 model at α=-1.5° and -4°. Fig. 9(a) showed power spectrum maps of 918+/-20 Hz. Fig. 9(b) showed coherence maps of 918 Hz. Fig. 9(c) showed phase delay map of 918 Hz. Reference point to calculate coherence and phase delay was selected as the pixel which had the largest power spectrum value at each test case. On fig. 9(a), distribution of the large power area was appeared near the trailing edge and it was moved toward the trailing edge according to the angle of attack from α=-1.5° to -4°. It agreed with the knowledge that smaller angle of attack increased positive pressure gradient and boundary layer transition went downstream. From power spectrum maps in fig. 9(a), dominant aerodynamic phenomena seemed 3-dimansional especially in α=-1.5° case, however, coherence maps in fig. 9(b) showed that discrete large power areas had large coherence value coh^2>0.5 and correlate with each other. Coherence data figured out that aerodynamic phenomena of α=-1.5° to -4° was 2-dimansional.

Fig. 9(c) showed phase delay maps of α=-1.5° to -4°. From phase delay maps, number of propagation waves in unsteady pressure fluctuation area was clearly measured. On the phase map of α=-1.5° in fig. 9(a), unsteady pressure area had 4 wavelength at the y/c=0 centerline, however, it had 3 wavelength at right and left area. Unsteady PSP measurement can produce unsteady information as image, relation between local part can be made clear. Comparing the angle of the phase delay on the x/c=0.9 line of α=-1.5° in fig. 9(a), y>0 right-hand side area was delayed one wavelength, 360°, than y<0 left-hand side area. about 0.5 wavelength, 180°, delayed than y>0 right-hand side area. These meant that phase of the unsteady information propagation was not uniform within unsteady pressure fluctuation area.

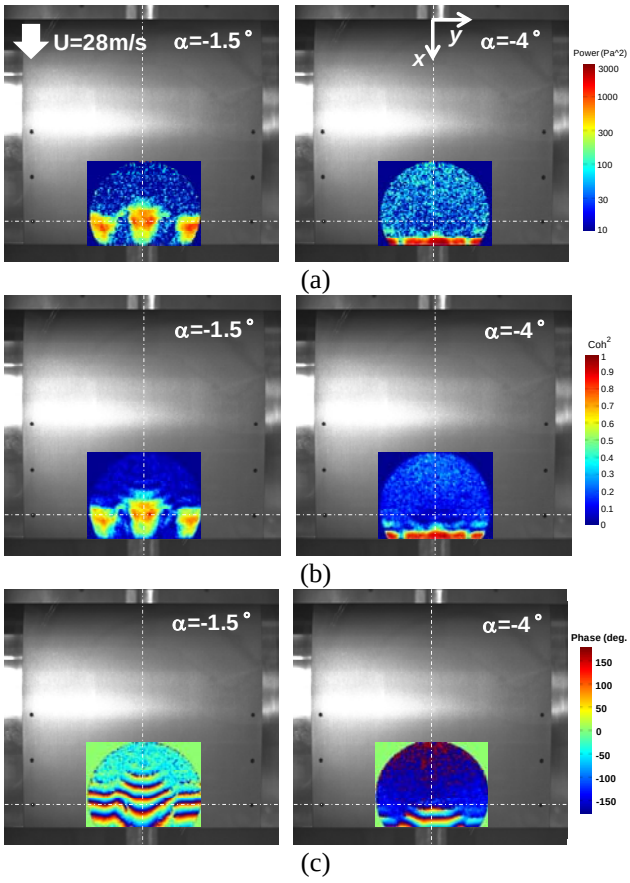

Fig. 9. Unsteady PSP measurement results on NACA 0012 model. (a) power spectrum of 918Hz+/-20Hz, (b) coherence of 918Hz, (c) phase delay of 918Hz at α=-1.5° and -4°.

4.2 30P30N Model

Aerodynamic noise caused by flow separation at the slat cove is known as one of the major components of the airframe noise. The shear

layer from the slat cusp reattaches to upstream of the slat trailing edge and causes a primarily broadband noise spectrum. However, the slat noise spectrum often exhibits narrowband peaks (NBPs) superimposed on the broadband spectrum especially in the case of two-dimensional unswept model configurations at lower than full-scale Reynolds numbers. Unsteady PSP measurement of the 2-dimensional 30P30N model was conducted at the flow speed U=58.0 m/s and α=0°, 3.5°, 6° to investigate aeroacoustic flow field of NBPs around the slat cove. Unsteady PSP results shown in this paper were angle of attack α=0° and 3.5°. Unsteady PSP measurement area was shown in fig. 10. 7W blue LD illumination area was about ϕ60mm circle inside red dashed line.

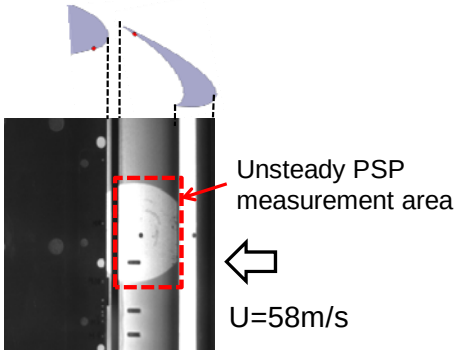

Fig. 10. Unsteady PSP measurement area on the slat of 30P30N model.

Fig. 11 showed PSD of Cp spectrum of α=0° and 3.5° measured by unsteady PSP measurement results. It can be confirmed that the PSD of Cp spectrum was consisted of broadband and NBPs superimposed on the broadband. 4 frequencies on each figure were fundamental, second harmonic, and two typical broadband frequencies. In 30P30N case, PSD of Cp was used to express unsteady power spectrum value.

Fig. 12 showed PSD of Cp, coherence , and phase delay maps of α=0° and 3.5° for 4 frequencies. Coherence and phase delay were calculated between one reference pixel with largest power and each pixel.

In fig. 12 (a) and (b), all of the figures in fig. 12(a) had higher value between reattachment line and trailing edge. Distribution of PSD of Cp between NBPs, 1420 and 2080 Hz, and broadband, 1800 and 2500 Hz, had little

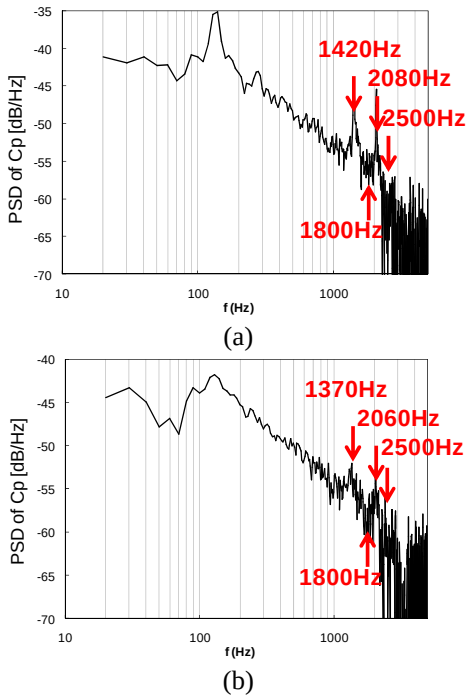

Fig. 11. Power spectrum density of Cp from unsteady PSP measurement. (a) α=0°, (b) α=3.5°.

difference, however, it was obviously observed that coherence distribution of NBP frequencies in fig. 12(b) had large spanwise correlation. On the other hand, broad band frequencies showed small correlation area. It was also confirmed that distribution of the phase delay of NBPs frequencies in fig. 12(c) was perpendicular to flow direction and uniform for spanwise. Those of broadband frequencies were random. Difference of the coherence caused quantitative difference of the aerodynamic noise of NBPs and broadband. Those of NBPs had 25-30 dB larger than that of broadband frequencies [24].

For the case of α= 3.5°, PSD of Cp distribution on all of the PSD of Cp maps in fig. 12(d) also had little difference but coherence maps had difference between NBPs, 1370 and 2060 Hz, and broadband, 1800 and 2500 Hz. However, coherence of NBPs frequencies of α=3.5° was different from α=0°. Coherence value and chordwise and spanwise broadening were larger than those of broadband frequencies, however they became smaller than those of α=0°. NBPs flow field of α=0° was extremely 2-dimensional. 2-dimansional structure started to break and get close 3-dimensional random flow structure at α=3.5°.

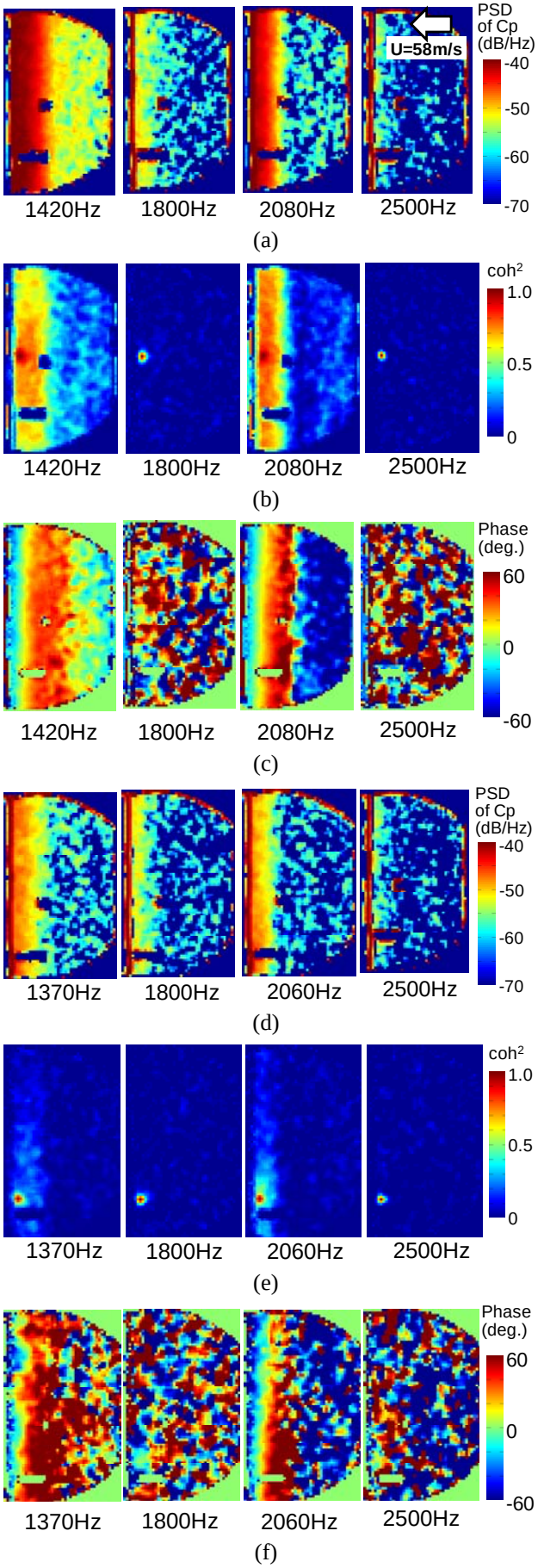

Fig. 12. Unsteady PSP measurement results on 30P30N model. (a) PSD of Cp map of α=0°, (b) coherence map of α=0°, (c) phase delay map of α=0°, (d) PSD of Cp map of α=3.5°, (e) coherence map of α=3.5°, (f) phase delay map of α=3.5°.

5 Conclusions

Unsteady PSP measurement system and FFT-based data reduction were introduced and two low-speed applications, NACA0012 and 30P30N model tests, and their results to extract unsteady flow filed information were described in detail.

In NACA0012 model test, aerodynamic phenomena was confirmed 2-dimansional from coherence information and local variation of the unsteady information propagation from phase delay information. In 30P30N model test, difference of coherence between NBPs and broadband and NBPs of α=0° and α=3.5° became clear from coherence information. Unsteady PSP measurement using a high-speed camera has high spatial resolution of less than 1 mm and it cannot be realized discrete unsteady pressure transducers so that these difference of flow phenomena became obvious in this paper. FF-based Unsteady PSP measurement would be a strong tool to understand unsteady flow filed and flow phenomena.

References

[1] Bell, J. H., Schairer, E. T., Hand, L. A., and Mehta, R. D., “Surface pressure measurements using luminescent coatings,” Annual Review of Fluid Mechanics, Vol. 33, 2001, pp. 155–206.

[2] Nakakita, K, Kurita, M, Mitsuo, K and Watanabe, S, Practical Pressure-Sensitive Paint Measurement System for Industrial Wind Tunnels at JAXA, *Measurement Science and Technology*, Vol.17, pp. 359-366, 2005.

[3] Asai K, Kanda H, Cunningham, C T, Erausquin, R and Sullivan, J, Surface Pressure Measurement in a cryogenic wind tunnel by using luminescent coating, International Congress on Instrumentation in Aerospace Simulation Facilities ’97 Record, pp.105-114, 1997..

[4] Sakaue, H, Sullivan, J P, Asai, K, Iijima, Y and Kunimasu, T, Anodized Aluminum Pressure Sensitive Paint in a Cryogenic Wind Tunnel, ISA

Proceedings of the 45th International Instrum. Sym., pp. 345-354, 1999.

[5] Sakaue, H, Tabei, T and Kameda, M, Hydrophobic monolayer coating on anodized aluminum pressure-sensitive paint, Sensors and Actuators B, Vol. 119, No. 2, pp. 504–511, 2006.

[6] Scroggin, A M, Slamovich, E B, Crafton, J W, Lachendo, N, Sullivan J P, Porous polymer/ceramic composites for luminescent-based temperature and pressure measurement, Proceedings of the Materials Research Society Symposium, Vol. 560, pp. 347–352, 1999.

[7] Kameda, M, Tabei, T, Nakakita, K, Sakaue, H and Asai, K, Image measurements of unsteady pressure fluctuation by a pressure-sensitive coating on porous anodized aluminium, *Measurement Science and Technology*, Vol.16, pp.2517–2524, 2005.

[8] Nakakita, K, Takama, Y, Imagawa, K and Kato, H, Unsteady PSP Measurement of Transonic Unsteady Flow Field around a Rocket Fairing Model, AIAA2012-2578, 2012.

[9] Merienne, M-C, Le Sant, Y, Lebrun, F, Deleglise, B and Sonnet, D, Transonic Buffeting Investigation using Unsteady Pressure-Sensitive-Paint in a Large Wind Tunnel, AIAA2013-1136, 2013.

[10] Michou, Y, Deleglse, B, Lebrun, F, Scolan, E, Grivel, A, Steiger, R, Pugin, R, Merienne, M–C, Le San, Y, Development of a Sol-Gel Based Nanoporous Unsteady Pressure Sensitive Paint and Validation in the Large Transonic ONERA's S2MA Windtunnel, AIAA 2015-2408, 2015.

[11] Sugioka, Y, Numata, D, Asai, K, Koike, S, Nakakita, K and Nakajima, T, Polymer/Ceramic PSP with reduced Surface Roughness for Unsteady Pressure Measurement in Transonic Flow, AIAA-2016-2018, 2016.

[12] Sugioka, Y, Nakakita, K and Asai, K, Non-intrusive Unsteady PSP Technique for Investigation of transonic Buffeting, Proceedings of ICAS-2016, 2016.

[13] Gregory, J W, Sullivan, J P, Wanis, S S and Komerath, N M, Pressure-sensitive Paint as a Distuributed Optical Microphone Array, *J. Acoust. Soc. Am.*, Vol. 119, pp.251-261, 2006.

[14] Yorita, D, Nagai, H and Asai, K, Unsteady PSP Technique for Measuring Naturally-Disturbed Periodic Phenomena, AIAA 2010-307, 2010.

[15] Nakakita, K, Unsteady Pressure Distribution Measurement around 2D-Cylinders Using Pressure-Sensitive Paint, AIAA-2007-3819, 2007.

[16] Nakakita, K, Unsteady Pressure Measurement on NACA0012 Model Using Global Low-Speed Unsteady PSP Technique, AIAA-2011-3901, 2011.

[17] Nakakita, K, Detection of Phase and Coherence of Unsteady Pressure Field Using Unsteady PSP Measurement, AIAA-2013-3124, 2013.

[18] Fang, S, Disotell, K J, Long, S R, Gregory, J W, Semmelmayer, F C and Guyton, R W, 2010, Application of Fast-Responding Pressure-Sensitive Paint to a Hemispherical Dome in Unsteady Transonic Flow, *Experiments in Fluids*, Vol. 50, No. 6, pp. 1495-1505, 2010.

[19] Seya, Y, Nishida, R, Kameda, M and Nakakita, K, Frequency Response of Fast-response Pressure Sensitive Paint with a Hydrophobic Coating, Proceedings of the 40th Symposium on Visualization, 2012. (in Japanese)

[20] Boll, S F, Suppression of Acoustic Noise in Speech Using Spectral Subtraction, *IEEE Transactions on Acoustics, Speech, and Signal Processing*, Vol. ASSP-27, No.2, pp.113-120, 1979.

[21] https://info.aiaa.org/tac/ASG/FDTC/DG/BECAN_files_/BANCII.htm (May 1, 2014).

[22] https://info.aiaa.org/tac/ASG/FDTC/DG/BECAN_files_/BANCII_category7/Summary_Category_7_Slat_Noise_30P30N.pdf (March 2014).

[23] Choudhari, M, Yamamoto, K, Integrating CFD, CAA, and Experiments towards Benchmark Datasets for Airframe Noise Problems, Proceedings of 5th Symposium on Integration CFD and Experiments in Aerodynamics (Integration 2012), 2012.

[24] Murayama, M, Nakakita, K, Yamamoto, K, Ura, H, Ito, Y, Choudhari, M, Experimental Study of Slat Noise from 30P30N Three-Element High-Lift Airfoil in JAXA Hard-Wall Low-Speed Wind Tunnel, AIAA-2014-2080, 2014.

[25] McAlpine A, Nash, E C and Lowson, M V, On the Generation of Discrete Frequency Tones by the Flow around an Aerofoil, *Journal of Sound and Vibration*, Vol. 222, Issue 5, pp. 753-779, 1999.

[26] Nash, E C, Lowson, M V and McAlpine, A, Boundary-layer instability noise on aerofoils, *J.Fluid Mech.*, Vol.382, pp. 27-61, 1999.

Contact Author Email Address

mailto:nakakita@chofu.jaxa.jp

Copyright Statement